HIGH C_x/C_o 13nm-CAPACITIVE-GAP TRANSDUCED DISK RESONATOR

Jalal Naghsh Nilchi, Ruonan Liu, and Clark T.-C. Nguyen
Department of Electrical Engineering and Computer Science
University of California at Berkeley, CA, USA

ABSTRACT

Electrode-to-resonator gaps as small as 13.2nm achieved on a 59.5-MHz capacitive-gap transduced disk resonator have now enabled a measured electromechanical coupling strength (C_x/C_o) greater than 1.62% at a bias voltage of only 5.5V while retaining an unloaded Q of 29,640, for a k_t^2Q product of 480 that sets the record at VHF. Several key discoveries contribute to this successful demonstration, including a modified polysilicon etch recipe that enables considerably smoother etch sidewalls than previously achievable, allowing more uniform sidewall sacrificial layer deposition and preventing structure pull-in by removing asperities and their associated strong electric fields. This combination of high (C_x/C_o) and Q stands to reduce power consumption in low-noise oscillators, improve sensitivity for zero-quiescent all-mechanical receivers, and expand the range of filters accessible to capacitive-gap transduced resonators to more mainstream wireless communication applications with much improved insertion loss performance.

INTRODUCTION

Capacitive-gap transduced resonators are well known to provide high on-chip Q's, with values reaching 150,000 at VHF [1] and 40,000 at 3GHz [2]. Q's this high enable 0.1% bandwidth channel-select filters with low insertion loss and high rejection [3] for ultra-low power transceivers [4]; as well as low-power, low-noise oscillators with best-in-class figure of merits on the order of -225dB [5]. Other characteristics that distinguish these resonators over alternatives include designable spurious mode suppression [3] and a voltage-controlled on/off self-switching capability [4] that allows realization of switchable filter [6] or oscillator [7] banks without the performance hit from series switches. At HF (from 3-30 MHz), capacitive-gap transduced resonators also post strong electromechanical coupling, as gauged by (C_x/C_o), up to 30% [8].

Despite these advantages, capacitive-gap transduced micromechanical resonators still struggle to realize the needed (C_x/C_o) values applicable to wider bandwidth filters centered at VHF or higher frequency, such as the 3% bandwidth ones used in existing smartphones. Higher (C_x/C_o) than the 0.1% attained in [3] are desirable for higher order channel-select filters using more than two resonator array-composites. For example, a 3-resonator filter works best with (C_x/C_o) ~ 0.25%; a 4-resonator with ~0.56%. To satisfy such (C_x/C_o) needs, recent efforts employ piezoelectric materials, but with significant reduction in Q and consequent increase in undesirable insertion loss to 8dB for 0.27% bandwidth, which is not acceptable right after the antenna in an RF front-end [12].

Alas, the path to higher (C_x/C_o) for higher Q capacitive-gap transduced devices is quite clear: Simply reduce the electrode-to-resonator capacitive gap [13]. As suggested by the simulation results of Fig. 2, a single wineglass disk resonator of Fig. 1 can achieve a (C_x/C_o) stronger than 1% and a motional impedance smaller than 100Ω by employing a 25nm gap spacing with a bias voltage V_P of 10V. Further reducing the gap to 10nm accompanied by 58V of V_P achieves a coupling strength of 6% at GHz frequency (*cf.* Table 2).

Although gap reduction via ALD partial-gap filling [14], [15] down to an effective 37nm confirmed the possibility of higher (C_x/C_o) ~0.58% for capacitive-gap transduced resonators, this is a far cry from what is possible. Indeed, one must ask the question, "What is the gap spacing limit?"

Pursuant to answering this question, this work demonstrates electrode-to-resonator gaps as small as 13.2nm

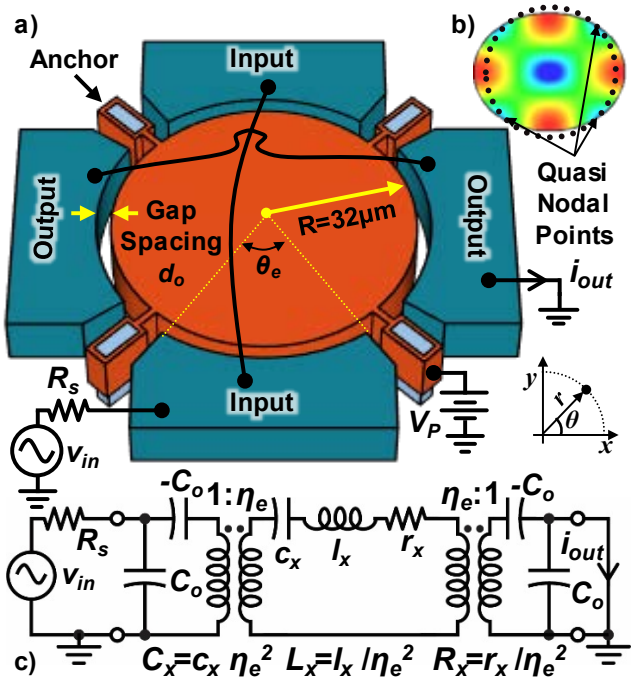

Fig. 1: (a) Illustration of a wine-glass disk resonator in a typical two port operation scheme. (b) Mode shape and quasi nodal points where the supports attach. (c) Electrical equivalent LCR circuit.

Table 1: Comparison between contour-mode AlN [9], quartz [10] and capacitive technologies at VHF.

	f_0 [MHz]	$\frac{C_x}{C_0}(k_t^2)$ [%]	R_x [Ω]	Q	k_t^2Q	Area [μm]²
[9]	85	0.86	125	2,100	18	10,000
[10]	149	0.48	460	10,000	48	21,200
This Work	60	1.62	54	29,640	480	3,200

Table 2: Projected performance as a function of gap spacing and dc-bias for 1-GHz capacitive-gap transduced resonators.

	d_0 [nm]	V_P [V]	$\frac{C_x}{C_0}(k_t^2)$ [%]	R_x [Ω]	Q	k_t^2Q
FBAR [11]	--	--	5.8	50	4,900	284
Cap. (Diamond) [2]	10	58	6.0	4.3	40,000	2400

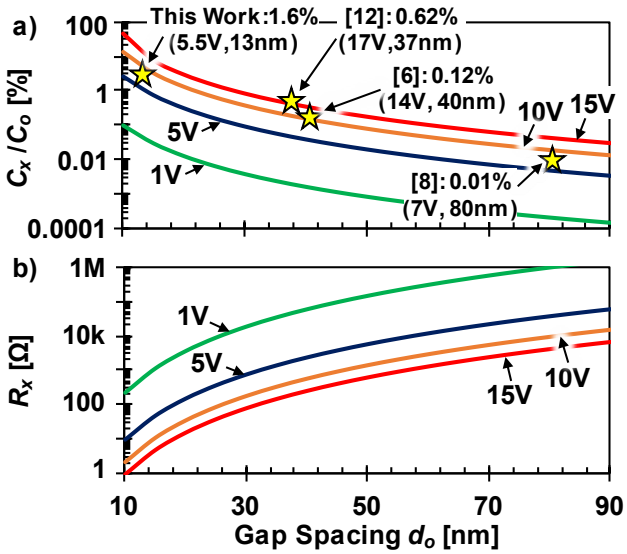

Fig. 2: Simulated plots of (a) electromechanical coupling strength (C_x/C_o) and (b) motional resistance R_x versus electrode-to-resonator gap spacing d_0 and bias voltage V_P for a 2μm-thick 60-MHz wineglass disk resonator with Q=70,000.

achieved on a 59.5-MHz capacitive-gap transduced disk resonator that yield a measured electromechanical coupling strength (C_x/C_o) greater than 1.62% at a bias voltage of only 5.5V, which together with an unloaded Q of 29,640 achieves a k_t^2Q product of 480 that far exceeds that of competitors, as shown in Table 1. This combination of high (C_x/C_o) and Q not only cuts a path towards power reduction for low-noise oscillators [5] and higher sensitivity for zero-quiescent all-mechanical receivers [16], but also expands the range of filters accessible to capacitive-gap transduced resonators to more mainstream wireless communication applications.

ELECTROMECHANICAL COUPLING COEFFICIENT (C_x/C_o)

The electromechanical coupling factor (C_x/C_o) gauges the efficiency of energy transfer between electrical and mechanical domains. It sets the upper bound on the percent bandwidth of a micromechanical filter [8], the tuning range of a capacitive-gap transduced resonator's center frequency [17], the sensitivity of capacitive microphones, and the efficiency of CMUT devices [18]. The electromechanical coupling factor for the capacitive-gap transduced wine-glass resonator shown in Fig. 1, defined as the mechanical energy relative to the total energy, takes the form

$$\frac{C_x}{C_o} = \varepsilon_o \cdot \frac{V_P^2}{d_o^3} \cdot \frac{R}{2\pi\rho\omega_o^2} \cdot \frac{\sin^2(\theta_e)}{\theta_e} \cdot \frac{R_m^2(R)}{\int_0^R R_m^2(r) r dr} \qquad (1)$$

where ε_o, V_P, d_o, ω_o, R, ρ, θ_e, $R_m(r)$ are vacuum permittivity, bias voltage, gap spacing, the disk radian resonance frequency, radius, density, electrode angle (*cf.* Fig. 1), and resonance mode shape function [19], respectively.

This expression makes very clear the importance of achieving a small electrode-to-resonator gap d_o for maximum (C_x/C_o), where a third power dependence makes gap spacing

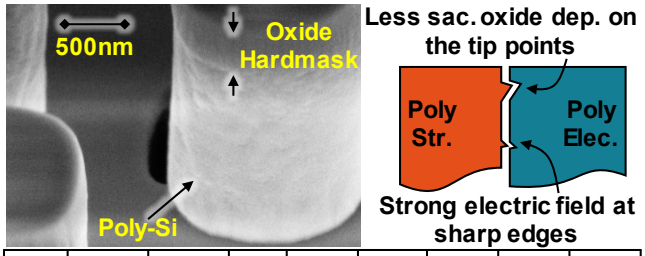

Step	TCP RF [W]	Bias RF [W]	Gap [cm]	HBr [sccm]	Cl_2 [sccm]	O_2 [sccm]	He [sccm]	CF_4 [sccm]
#1	200	40	6.03	0	0	0	0	100
#2	250	55	6.03	150	4	1	4	0

Fig. 3: Practical considerations indicated at top right demand polySi sidewall smoothness on the same order or smaller than the sidewall sacrificial film thickness. The LAM TCP 9400SE etcher recipe summarized in the table achieves a very smooth surface, shown in the SEM above. Here, step #1 breaks through any native oxide, then successive cycles of processing/cooling of step #2 etch the polySi.

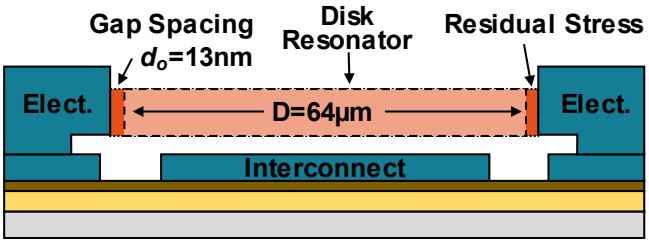

Fig. 4: Illustration depicting how residual stress can cause shorts between disk and electrode when the gap becomes very small.

the strongest control knob by far. Note that (1) correctly predicts that capacitive-gap transducers with gaps of 100nm already exhibit coupling strengths that outperform AlN piezoelectrics at HF (up to 30MHz) [8]. To outperform AlN above VHF, smaller gaps are needed. For example, at GHz frequencies gaps below 20nm are desirable, *cf.* Table 2.

NANOSCALE GAP SPACING

Inevitably, benefits afforded by scaling generally come with consequences. In particular, a shrinking electrode-to-resonator gap invites numerous possible issues, including

1) Asperities in the gap sharp enough to concentrate electric fields to the point of breakdown (*cf.* Fig. 3).
2) Asperities that reduce the effective gap distance, disturbing the force balance on opposite sides of the disk, and thereby lowering the pull-in voltage.
3) Compressive film stress caused by slower shrinkage of the disk with decreasing temperature relative to the substrate that effectively stretches the disk edges into contact with the surrounding electrode, as shown in Fig. 4.
4) Popular issues of folklore, such as Casimir forces, electric field limits before breakdown, e.g., 1V/nm, etc.
5) Obstructions in the gap, e.g., from condensation.

Each of the above, of course, are inter-related. In particular, compressive stress issues amplify if there are asperities, which arguably puts surface roughness among the most disruptive issues. Recognizing this, the fabrication process to

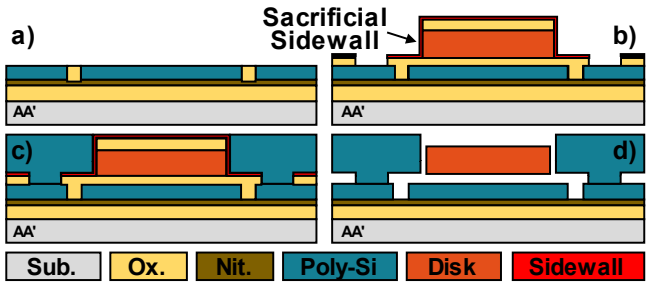

Fig. 5: Fabrication process yielding tiny-gap resonators.

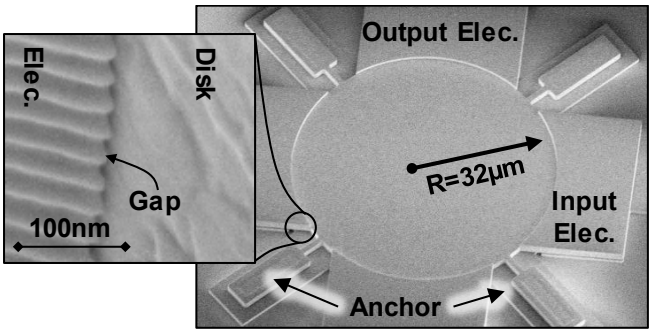

Fig. 6: SEM of a released wineglass disk resonator with zoom-in to highlight the smooth structure etch compared to the standard high-selectivity electrode etch.

achieve sub-20nm gaps puts particular importance on attaining as smooth and straight sidewalls as possible.

Fig. 5 summarizes the fabrication process yielding the Fig. 1 disk resonator. The process begins with blanket LPCVD depositions of oxide and nitride to form an isolation layer, followed by LPCVD oxide deposition and patterning to form a mold into which doped polysilicon is deposited then CMP'ed down to yield thick, low-resistance interconnect, as shown in (a). The resultant flat surface after CMP'ing facilitates subsequent blanket LPCVD of bottom sacrificial oxide, structural polysilicon, and top oxide hard mask, the last two of which are patterned and etched to delineate the disk. To suppress issue 3 above, this work employs polySi deposited at 590°C and annealed at 1000°C for 30min to achieve very low residual stress (5MPa) and near-zero stress gradient, both much smaller than the critical values of 60MPa and 50MPa/μm, respectively, that could otherwise cause shorts.

It is here where the carefully designed etch recipe summarized in Fig. 3 makes all the difference in the ability to achieve sub-20nm gaps. Specifically, the HBr-based polySi etch is anisotropic and yields a smoother sidewall than a Cl_2-based etch, since the etch rate depends less on the silicon crystalline orientation and polySi grain boundaries.

The smooth sidewalls devoid of asperities larger than 10nm high now facilitate deposition of the gap-setting sidewall sacrificial oxide down to 10 nm via LPCVD at 930°C. Patterning and etching of electrode anchors follows to yield the cross-section of (b). Subsequent polySi deposition and doping, followed by CMP and electrode patterning and etching then yield the planarized cross-section of (c). Finally, wet-etching in 49% HF yields the released resonator of (d).

Fig. 6 presents the SEM micrograph of a released wineglass disk resonator with zoom-in on the electrode-to-resonator overlap. Here, the smooth-sidewall structure achieved by the Fig. 3 etch recipe contrasts sharply with the much rougher electrode etch done via a conventional SF_6-based chemistry aimed more at higher polysilicon-to-oxide selectivity.

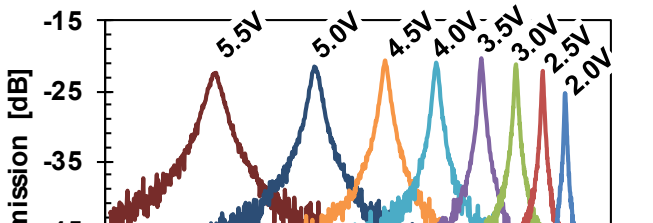

Fig. 7: Measured frequency response of the WG disk resonator for various V_P's. With 3.0V bias, the unloaded Q is 29,640 with a motional resistance of 200Ω. The Q decreases at higher voltages when the motional resistance of the device becomes significantly smaller than that of the polySi interconnect, suggesting that metal interconnect be used in future devices to prevent this Q reduction.

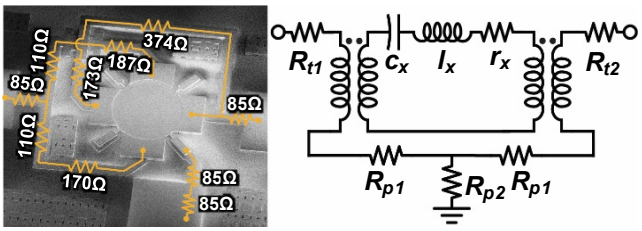

Fig. 8: Trace resistance on the input/output path as well as the bias path can load the resonator and degrade its quality factor Q.

EXPERIMENTAL RESULTS

Fig. 7 presents the vacuum-measured frequency response of the fabricated wineglass disk of Fig. 1 for various bias voltages V_P. The unloaded Q of this resonator is 29,640, measurable at 10μTorr and with small V_P. As V_P increases, R_x shrinks to only 54Ω at V_P=5.5V, which is considerably smaller than the 750Ω interconnect resistance (*cf.* Fig. 8), allowing the latter to load the overall Q down to 2,500. Thus, preservation of the unloaded resonator Q of 29,640 in future devices calls for much lower interconnect resistance, perhaps provided by metals.

Replotting the data of Fig. 7 as frequency versus V_P yields Fig. 9(a), from which curve-fitting [17] accurately extracts a remarkable 13.2nm electrode-to-resonator gap spacing. As evident from this figure, the 59.5MHz-wineglass resonator has more than 1MHz of tuning range for only 5.5V of biasing voltage, all consistent with the expected increase in electrical stiffness with decreasing gap spacing. The electrical stiffness at 5.5V is 23.4kN/m, which is 3.05% of the disk's 766.5kN/m mechanical stiffness.

The electromechanical coupling factor (C_x/C_o) was extracted from measured frequency response curves using an

expression derived from the electrical circuit of Fig. 1:

$$\frac{C_x}{C_o} = \frac{f_p^2 - f_s^2}{f_s^2} \times 100 \qquad (2)$$

where f_s and f_p are the series and parallel resonance frequencies, respectively, of the transmission measurement. Fig. 9 (b) plots (C_x/C_o) versus bias voltage, showing an impressive (C_x/C_o) of 1.6% at 5.5V bias, which matches the prediction of (1) using the measured gap spacing.

To address concerns about the linearity of a capacitive-gap transducer with such a tiny gap, the two-tone nonlinearity measurement summarized in Fig. 10 reveals third-order intercept points (IIP3's) of +23dBm and +29dBm for tone spacings of 580kHz and 3MHz, respectively, both already adequate for today's cellular handsets, and if even needed, with room for improvement via mechanical coupled arraying [20].

CONCLUSION

By demonstrating the first true sub-20nm capacitive-gap VHF micromechanical disk resonator to meet the simultaneous high Q (29,640), low motional resistance R_x (54Ω), and high electromechanical coupling C_x/C_o (1.62%), this work fixes a common misconception among RF MEMS researchers that capacitive-gap transducers are weaker than piezoelectric counterparts. The achieved and projected performances summarized in Table 1 and Table 2, respectively, further shows that the resonator demonstrated herein outperforms competitors in all respects, especially in the popular k_t^2Q product metric. This combination of high (C_x/C_o) and Q, which has long been a primary driver for RF MEMS research, stands to not only cut VHF low noise oscillator power consumption to sub-µW levels, but now creates opportunities to apply MEMS resonator technology to the highly profitable and lucrative RF filter market for smartphones, where gaps of 10nm with higher bias voltage should allow the 6% C_x/C_o's at GHz frequencies needed for such filters, *cf.* Table 2.

ACKNOWLEDGEMENT: This work was supported by DARPA.

REFERENCES

[1] M. A. Abdelmoneum *et al.*, "Stemless wine-glass-mode disk micromechan…," DOI: 10.1109/MEMSYS.2003.1189845.

[2] T. L. Naing *et al.*, "2.97-GHz CVD diamond ring resonator with Q >40,000," DOI: 10.1109/FCS.2012.6243723.

[3] M. Akgul *et al.*, "A passband-corrected high rejection channel-select …," DOI: 10.1109/FCS.2014.6860009.

[4] C. T.-C. Nguyen, "MEMS-based RF channel selection for true software- …," DOI: 10.1109/MCOM.2013.6495769.

[5] T. L. Naing *et al.*, "A 78-microwatt GSM phase noise-compliant …," DOI: 10.1109/EFTF-IFC.2013.6702305.

[6] S.-S. Li *et al.*, "Self-switching vibrating micromechanical filter bank," DOI: 10.1109/FREQ.2005.1573915.

[7] T. L. Naing *et al.*, "Simultaneous multi-frequency switchable oscillator and …," DOI: 10.1109/MEMSYS.2015.7051136.

[8] J. Naghsh Nilchi *et al.*, "7th order sharp-roll-off bridged micro- …," DOI: 10.1109/TRANSDUCERS.2015.7180880.

[9] G. Piazza *et al.*, "Piezoelectric Aluminum Nitride Vibrating Contour-Mode …," DOI: 10.1109/JMEMS.2006.889503.

[10] D. T. Chang *et al.*, " A New MEMS-Based Quartz Resonator Technology," in *Hilton Head*, 2004.

[11] R. Ruby *et al.*, "Method of Extracting Unloaded Q Applied Across Different …," DOI: 10.1109/ULTSYM.2008.0446.

[12] G. Piazza *et al.*, "Single-Chip Multiple-Frequency ALN MEMS Filters …," DOI: 10.1109/JMEMS.2006.889503.

[13] C. T.-C. Nguyen, "RF MEMS for Channelizing Low-Power Radios," DOI: 10.1109/Transducers.2013.6627303.

[14] M. Akgul *et al.*, "Capacitively transduced micromechanical resonators w/ simultaneous low …," in *Hilton-Head,* 2010.

[15] T. J. Cheng *et al.*, "High-Q, low impedance polysilicon resonators with …," DOI: 10.1109/MEMSYS.2010.5442311.

[16] R. Liu *et al.*, "Zero quiescent power VLF mechanical comm …," DOI: 10.1109/TRANSDUCERS.2015.7180878.

[17] M. Akgul *et al.*, "A negative-capacitance equivalent circuit model for parallel-…," DOI: 10.1109/TUFFC.2014.2976.

[18] G. G. Yaralioglu *et al.*, "Calculation and measurement of electromechanical …," DOI: 10.1109/TUFFC.2003.1197968.

[19] Y.-W. Lin *et al.*, "Series-resonant VHF micromechanical resonator reference …," DOI: *10.1109/JSSC.2004.837086.*

[20] J. Naghsh Nilchi *et al.*, "Third order intermodulation distortion in …," DOI: 10.1109/FCS.2015.7138782.

CONTACT: J. Naghsh Nilchi, jnnilchi@eecs.berkeley.edu

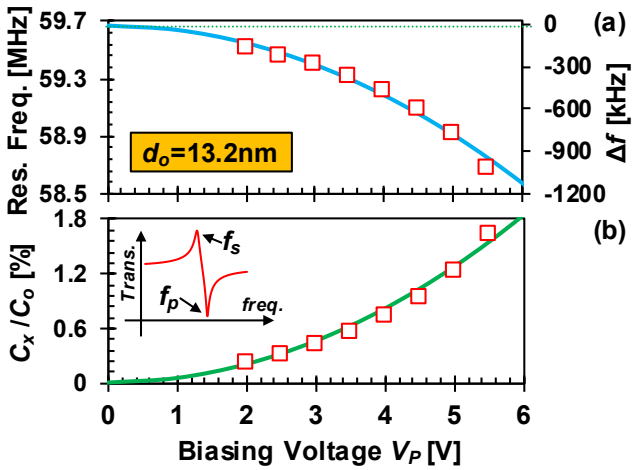

Fig. 9: 10µTorr-vacuum-measured (a) resonance frequency and (b) electromechanical coupling (C_x/C_o) for a 13.2nm-gap WG disk determined using series f_s and parallel f_p resonance frequencies, both plotted against bias voltage V_P.

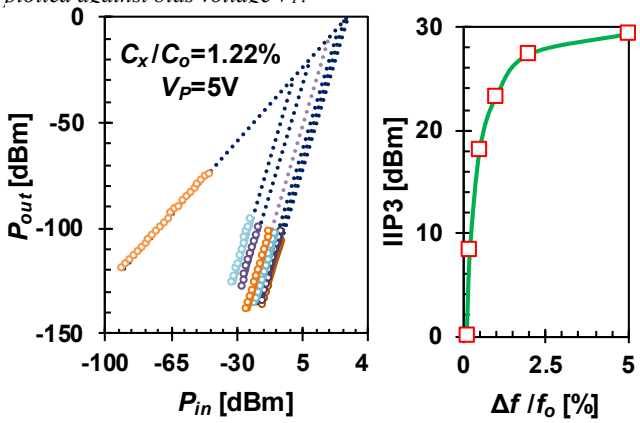

Fig. 10: Two-tone nonlinearity measurement of the 13.2nm-gap WG disk and plot of IIP3 versus tone offset from the center frequency.